GROWTH OF TURBULENT SPOTS IN HIGH-SPEED BOUNDARY LAYERS

Andreas Jocksch* **and Leonhard Kleiser**
Institute of Fluid Dynamics
ETH Zurich
8092 Zurich, Switzerland
*jocksch@ifd.mavt.ethz.ch

ABSTRACT

In this contribution we investigate the development of turbulent spots in supersonic boundary layers by means of direct numerical simulations. The spot structure is analysed and mean velocity profiles and Reynolds stresses are determined applying ensemble averaging over many simulations. The near field of the spots reveals waves propagating away from the spot in semi-circular patterns. Spot characteristics such as the approximate self-similarity and the resulting spreading angle and effects of Mach and Reynolds numbers are discussed and compared with results from literature.

INTRODUCTION

The occurrence of turbulent spots in laminar flow was reported in early transition experiments (Emmons, 1951; Schubauer and Klebanoff, 1955). The transition process is described as a randomly distributed emergence of turbulent spots which initially grow linearly. They subsequently merge and develop into turbulent flow. The assumption of approximate linear growth characteristics of the spot (also called self-similarity) together with its random distribution function has been taken as a basis for transition modelling. In order to obtain knowledge about their spreading mechanism, the growth of individual turbulent spots has been investigated. Simulations for incompressible boundary layers (see e.g. Breuer and Haritonidis, 1990; Singer and Joslin, 1994, among others) provided details about the flow structure of turbulent spots.

Turbulent spot growth in high-speed boundary layers has been studied far less frequently. The influence of the Mach number on spot growth has been discussed based on experimental results (Fischer, 1972; Fiala et al., 2006) but not finally explained. Recently, direct numerical simulations (DNS) of spot growth in compressible boundary layers were performed by Krishnan and Sandham (2006a,b, 2007). In the present contribution, we study the growth of turbulent spots in laminar boundary layers at different Mach numbers also by means of DNS. After briefly describing the numerical approach we present an analysis of a transitional boundary layer with respect to spot structure and turbulence statistics. The analysis is continued by investigating the Mach number effect on spot growth. The near field of turbulent spots is investigated and the growth is quantified and compared with the literature.

SIMULATION METHODOLOGY

Supersonic isothermal-wall boundary layers on a flat plate with a wall temperature equal to the adiabatic laminar boundary-layer solution are considered. At the outer edge of the computational domain non-reflecting boundary conditions are applied. Dirichlet boundary conditions with sponge zones are used at the inflow and outflow boundaries. In the spanwise direction periodicity is applied. To specify the initial and boundary conditions a boundary-layer similarity solution according to Howarth-Dorodnitsyn (Stewartson, 1964) is used. At moderate Reynolds numbers, differences between the boundary-layer approximation and the Navier-Stokes solution exist which are on the order of the small physical disturbances present in our simulation. Therefore, in our simulations a forcing term is applied to the Navier-Stokes equations that maintains the laminar boundary layer solution when no disturbances are present.

A sixth-order compact finite-difference scheme (Lele, 1992) is used for spatial discretisation and a low-storage third-order Runge-Kutta method (Williamson, 1980) or the classical forth order Runge-Kutta method are employed for time-marching. The convective terms are expressed in skew-symmetric form following Honein and Moin (2004) to enhance numerical stability. The viscous terms are expanded to damp grid-to-grid oscillations.

A vortex pair (emulating an oscillating membrane) is superimposed on the laminar boundary-layer solution to specify the initial disturbance. In the present study we adopt the disturbance definition used by Breuer and Haritonidis (1990) for triggering spots in incompressible flat-plate boundary layer flow,

$$\Psi = \epsilon \cdot (x/l_x)(y/l_y)(z/l_z)^3 e^{-(x/l_x)^2-(y/l_y)^2-(z/l_z)^2} \tag{1a}$$

$$(\rho u)' = 0,\ (\rho v)' = \Psi_y,\ (\rho w)' = -\Psi_z \tag{1b}$$

(triggering disturbance). The dimensions of the vortex pair in terms of the boundary layer displacement thickness are $l_x = 10/3$, $l_y = 4$, $l_z = 4/5$ and the strength is $\epsilon = 1$ for all simulations where (x, y, z) and (u, v, w) are the coordinates and velocities, respectively, in the streamwise, spanwise and wall-normal directions. Variables are non-dimensionalised with the freestream velocity U_∞ and the displacement thickness δ_1 at the triggering position of the spot.

We start with considering a transonic boundary layer transition at $M = 1.1$, $Re = 800$ denoted by case A1. Here the Reynolds number is defined by $Re = U_\infty \delta_1/\nu_\infty$ with values taken at the triggering position. Box dimensions and resolutions are given in Table 1. Due to the lack of any temporal or spatial homogeneity statistical properties are determined by averaging ensembles of different realisations of the spot. For this purpose the spots are triggered by superimposing small random disturbances to the vortex pair disturbing the laminar boundary-layer solution. The random noise has a homogeneous isotropic energy spectrum with a Fourier amplitude distribution according to

$$|\hat{u}_n| = |\hat{v}_n| = |\hat{w}_n| = \frac{1}{4000}\left(\frac{|K|}{k_p}\right)^8 \exp\left[-2\left(\frac{|K|}{k_p}\right)^2\right] \tag{2}$$

($|K|$ = wavenumber magnitude, $k_p = 4.2$). The phases of the Fourier modes were chosen randomly (distributed uni-

Table 1: Flow and simulation parameters.

	M	Re	L_x	$L_y/2$	L_z	N_x	N_y	N_z
A1	1.1	800	175	37.5	37.5	767	384	195
A2	1.1	1500	175	37.5	37.5	1580	385	385
B1	5.0	3000	250	54	37.5	1116	294	294
B2	5.0	5000	210	51	37.5	1900	525	595
C	5.0	800	210	37.5	37.5	988	207	299

formly over $[0, 2\pi)$) and for each simulation the collectivity of the phases comprises an independent uniform distribution. The homogeneous noise is modulated with the initial disturbance of the vortex pair, resulting in

$$(\rho u)'(u_n + 1), (\rho v)'(v_n + 1), (\rho w)'(w_n + 1) \qquad (3)$$

as the actual disturbance imposed. In this way the noise only affects the main disturbance (but not the surrounding laminar flow) and is made inhomogeneous, realising especially the zero velocity at the wall. The slight spanwise asymmetry of the spots generated in this manner is used to double the statistical sample size by averaging over spanwise mirror positions.

SPOT GROWTH

The initial disturbance is strong enough to cause a fast development into a turbulent spot. The spot grows locally without creating significant disturbances far from its centre (Smaller initial disturbances at moderate Reynolds number may extend over the whole computational domain before becoming turbulent).

Figures 1-3 show iso-contours of the wall-normal vorticity ω_z and of the second invariant λ_2 (see Jeong and Hussain (1995)) for case A1. The spot shows the typical properties such as the lifted tip, elongated streamwise structures in the tail region and an arrowhead-like plan-view shape. Comparing the visualisations of ω_z at different times gives insight into the disturbance development. Starting from the elongated structures at early times a breakdown occurs and a turbulent region is established. At the tail of the spot the primary elongated structures are maintained and multiply. No primary hairpin vortex of the type reported by Singer and Joslin (1994) and Krishnan and Sandham (2006a) is visible immediately after triggering. This is seen as the result of the different triggering procedure (in these previous studies a blow mechanism was employed to trigger turbulent spots). However, at a later stage a vortex system on the tip appears like in Singer and Joslin (1994). Our results look very similar compared to the incompressible case (Breuer and Haritonidis, 1990).

Figure 4 shows Favre-averaged streamwise velocity profiles in the mid-plane. The difference between the laminar profile and the spot region is clearly visible. The logarithmic region is only partially developed at this stage of transition. Disturbances are shown by means of the streamwise Reynolds normal stress $\bar{\rho}\widetilde{u''u''}$ in Figure 5. Strong fluctuations are visible in the core of the spot and at the lateral tails, whereas in the region of the tip vortex system the fluctuations are rather small. The Reynolds shear stress $-\bar{\rho}\widetilde{u''w''}$ (Figure 6) has its maxima at the same locations.

HIGHER MACH AND REYNOLDS NUMBERS

Apart from the transonic boundary layers at $M = 1.1$ (case A1) discussed previously we also consider supersonic boundary-layer flows at $M = 5$ (case B). Reynolds number effects are considered at both Mach numbers: The cases A1 and B1 are complemented by the corresponding cases A2 and B2 at higher Reynolds numbers. Furthermore, we investigate the effect of wall cooling at $M = 5$ at moderate Reynolds number (case C). Table 1 summarises the respective flow and simulation parameters. In contrast to case A1 we apply a spanwise-symmetry condition at the mid-plane $y = L_y/2$ in all other cases. On the one hand, this suppresses any asymmetric flow structures. On the other hand, the saving of computational effort allows to consider other spot features of particular interest, e.g. the near field. Experiments and simulations with broken symmetry (such as case A1 in the present contribution or Levin (2005)) indicate that turbulent spots are likely to develop in a symmetric manner. No noise is imposed in cases A2-C.

We first consider the transonic flow case A2. An increase of the Reynolds number at the triggering position leads to an enhanced growth of the spot and results in a larger extent of the spot at an earlier time (Figure 7) compared to the lower Reynolds number case (Figure 3). A similar phenomenology is found for spots in the high-supersonic regime (Figures 8, 9) which will be discussed below.

Straightforward comparisons of results at different Mach numbers are difficult. The desirable choice of an equal Reynolds number would raise the question of how to choose the reference viscosity (freestream or at the wall) and the reference length (e.g. displacement or momentum thickness). These quantities show a different ratio when the Mach number changes. For the present investigation, the Reynolds number has been chosen heuristically to provide a similar development of the disturbance (all boundary layers are significantly linearly unstable). A similar problem arises for the triggering procedure (Eq. (1)) which delivers the desired results but e.g. the size of the vortex pair could in principle also be related to a reference other than the displacement thickness.

Unlike in the transonic case, at high Mach number dominant spanwise structures close to the wall are present during the whole transition process. They have been observed also by Krishnan and Sandham (2006a) in their $M = 6$ case and have been associated with the presence of a Mack mode. Starting from the tip of the spot the spanwise structures decrease in magnitude towards the tail (Figure 8 bottom and mid-plane view). They are large and ordered compared to the typical hairpin vortices. Due to the presence of the spanwise-directed structures, hairpins (visible in the top view) are located away from the wall. The phenomenon is seen as a purely transitional one. Our simulation at higher Reynolds number shows more-turbulent behaviour at the wall (see bottom view of case B2, Figure 9). At the tip streamwise structures are dominant but degenerate towards the centre of the spot. Investigations of fully developed compressible turbulent boundary layers (e.g. Maeder et al., 2001) and wave-induced transition (Adams and Kleiser, 1996) have not indicated any dominance of large-scale spanwise structures.

One explanation of the different boundary-layer properties in dependency of Mach number can be given by linear stability theory. In general instabilities in boundary layers have large amplitudes in specific critical layers where the linear eigensolution phase velocity equals the velocity of the

base flow (Maslowe, 1986). For the transitional $M = 1.1$ case the least stable mode is a viscous one similar to a Tollmien-Schlichting wave with an oblique orientation. At $M = 5.0$ the so-called Mack mode is dominant, i.e. a second inflectional (inviscid) two-dimensional mode. The corresponding critical layer is located farther away from the wall than that of the dominant mode of the transonic boundary layer. The Mack mode shows acoustic behaviour at the wall and vortical one at the critical layer. Wave-induced transition based on this mode has been investigated by Adams and Kleiser (1996). As far as the properties of the laminar flow continue into the transitional region for the $M = 5$ case the Mack mode can be associated with the observed structures as claimed by Krishnan and Sandham (2006a). High vorticity close to the critical layer leads to small-scale structures whereas pressure fluctuations close to the wall generate large-scale spanwise structures in a more ordered way. An estimate of the wavelength and comparison to inviscid solutions (Mack, 1984) suggests the presence of a higher than second mode. A further aspect is the steep temperature gradient at a large distance from the wall. In a turbulent boundary layer it can feed the large temperature fluctuations which are dominant there. Large temperature fluctuations are predicted by Morkovin's hypothesis and have been previously confirmed by Maeder et al. (2001) using DNS. Together with the locally smaller viscosity these effects dominate compared to the region of steepest velocity gradient close to the wall. The turbulent motion is fed in the region of large temperature gradient leading to the presence of a wide range of scales of motion associated with various structures. Close to the wall fluctuations are driven by high velocity gradients but high viscosity permits large-scale motion only, as is observed with the spanwise structures. Further downstream mixing leads to large temperature gradients closer to the wall and the effect becomes weaker.

In order to investigate the effect of wall temperature, the simulation C has been performed with a cooled wall in which the wall temperature is set equal to the free-stream temperature. The iso-surfaces of λ_2 (Figure 10) show a different spot shape compared to the adiabatic wall case (Figures 8, 9). The effect of spanwise structures close to the wall is more pronounced than in case B1. Typical turbulent structures are just about to develop at this time instant.

NEAR FIELD OF TURBULENT SPOTS

A widely discussed point is the occurrence of waves in conjunction with turbulent spots. Wygnanski et al. (1979) found waves on the tail which generated new spots. Only a fraction of later investigations confirmed the existence of waves following the spot (Singer, 1996). An evaluation of the characteristics of the near field might bring insight into this aspect. The iso-contours of λ_2 in Figures 3 and 7-9 show semi-circular patterns reminiscent of disturbances propagating away from a point source. This effect appears more dominant for the high Reynolds number simulations (Figures 7, 9 (cases A2, B2)) than for lower Reynolds numbers (Figures 3, 8 (cases A1, B1)) at the specific λ_2 iso-value chosen. The downstream-propagating disturbances originate from the turbulent region of the spot. The vortex system at the tail moves with the spot but does not emit disturbances. The semi-circular wave pattern with some irregularities appears to be dominated by one mode, accompanied by further, possibly subharmonic modes of smaller magnitude. Note that the waves originating from periodic neighbours of the spot interact with each other and create interference patterns (see Figures 7, 8). For case B2 the dominant wavelength is smaller than of the least stable second-mode instability according to inviscid theory (Mack, 1984). These observations, which are different from those of Wygnanski et al. (1979) may be attributed to differences in characteristic parameters such as the Mach number. At early stages the waves can be attributed to the primary vortex system not being fully turbulent, while at later stages the spreading structures clearly emanate from the core of the turbulent spot. Our study differs from most of the previous investigations, in which no waves were shown surrounding the spot, by the presence of significant compressibility effects. However, the discrepancy in observing the presence of waves might perhaps also be explained by the weakness of the effect. The existence of propagating waves in the vicinity of the spot can be expected if some linear eigensolution exists with a group velocity larger than the propagation speed of the border of the spot. In any case disturbances radiate from the spot into the near field since turbulence radiates noise in general. There is no indication of the creation of new turbulent spots by the surrounding waves. The growth of radiated disturbances and subsequent breakdown into turbulence appears possible but was not observable within our limited computational domain. It has been discussed in the literature whether the spreading of turbulent spots can be associated with a wave-induced transition scenario. Within the relatively small area of waves surrounding the turbulent spots no analogy between the turbulent spot growth and wave-induced transition scenarios can be established.

SPOT GROWTH RATES

Early experiments (see e.g. Emmons (1951)) report a self-similarity of turbulent spots based on a linear growth of the spot size which is quantified by its constant spreading angle. Based on experimental results, Fischer (1972) showed a reduction of the growth rate with increasing Mach number. The spot growth in our simulations has been estimated in the time frame between the onset of turbulence and the end of the computations and self-similarity can be confirmed within a certain accuracy. The spot edges have been arbitrarily defined by $\omega_z = \pm 0.1$ iso-values. The spreading half-angles estimated from our spot simulations are shown in Figure 11, confirming the tendency of decreasing spreading angles with increasing Mach number. However, it must be mentioned that according to our simulations the Reynolds number at the triggering position also has a strong influence on the observed spreading. This is an effect known from parallel (fixed Reynolds number) flows such as plane Couette flow (Lundbladh and Johansson, 1991) but needs further clarification for growing boundary layers with continuously increasing Reynolds number. It is likely that the Reynolds numbers range in Fischer (1972) (the values are not documented) is higher than in our simulations and thus presumably lead to more perfect linear growth. Reynolds number effects are only one possible reason for the different spreading rates seen in the experimental results: other parameters such as freestream turbulence might have an influence as well. The correlation of Fischer (1972) is based on a limited variety of experiments. A wider range of spreading angles appears possible and may explain some discrepancies between simulations and experiments. An estimate of the growth rate for the cooled wall simulation (case C) is small compared to the adiabatic case B. This suggests stronger Mach number effects on the spot growth for non-adiabatic boundary layers.

Note that for the related case of a point source disturbance within a compressible boundary layer (Balakumar and Malik, 1992) spreading angles similar to those of turbulent spots (Fischer, 1972) have been determined.

CONCLUSIONS

Simulations of turbulent spots growing in supersonic boundary layers have been performed. At high Mach number the transition process within the boundary layer proceeds at a certain distance from the wall first. Close to the wall a sublayer exists where disturbances are only weak. It has been shown for all Mach and Reynolds numbers investigated that turbulent spots generate disturbances which propagate away in the streamwise and lateral directions, forming semicircular wave patterns. The investigation of a cooled wall revealed a multitude of large corrugated vortical structures together with distinct streamwise elongated structures at the onset of transition. Self-similarity of the spot growth described in the literature could be largely confirmed. The spreading angles lie within or close to the experimental range (Fischer, 1972), Figure 11.

ACKNOWLEDGEMENT

Computations were performed at the Swiss National Supercomputing Centre (CSCS).

REFERENCES

Adams, N. A., and Kleiser, L., 1996, "Subharmonic transition to turbulence in a flat-plate boundary layer at Mach number 4.5", *Journal of Fluid Mechanics*, 317:301–335.

Balakumar, P., and Malik, M. R., 1992, "Waves produced from a harmonic point source in a supersonic boundary-layer flow", *Journal of Fluid Mechanics*, 245:229–247.

Breuer, K. S., and Haritonidis, J. H., 1990, "The evolution of a localized disturbance in a laminar boundary layer. Part 1. Weak disturbances", *Journal of Fluid Mechanics*, 220:569–594.

Emmons, H. W., 1951, "The laminar-turbulent transition in a boundary layer. Part I", *Journal of the Aeronautical Sciences*, 18:490–498.

Fiala, A., Hillier, R., Mallinson, S. G., and Wijesinghe, H. S., 2006, "Heat transfer measurement of turbulent spots in a hypersonic blunt-body boundary layer", *Journal of Fluid Mechanics*, 555:81–111.

Fischer, M. C., 1972, "Spreading of a turbulent disturbance", *AIAA Journal*, 10(7):957–959.

Honein, A. E., and Moin, P., 2004, "Higher entropy conservation and numerical stability of compressible turbulence simulations", *Journal of Computational Physics*, 201:531–545.

Jeong, J., and Hussain, F., 1995, "On the identification of a vortex", *Journal of Fluid Mechanics*, 285:69–94.

Krishnan, L., and Sandham, N., 2006a, "Effect of Mach number on the structure of turbulent spots", *Journal of Fluid Mechanics*, 566:225–234.

Krishnan, L., and Sandham, N., 2006b, "On the merging of turbulent spots in a supersonic boundary-layer flow", *International Journal of Heat and Fluid Flow*, 27:542–550.

Krishnan, L., and Sandham, N., 2007, "Strong interaction of a turbulent spot with a shock-induced separation bubble", *Physics of Fluids*, 19:016102–1–11.

Lele, S. K., 1992, "Compact finite difference schemes with spectral-like resolution", *Journal of Computational Physics*, 103:16–42.

Levin, O., 2005, *"Numerical studies of transition in wall-bounded flows"*, PhD thesis, KTH, Stockholm.

Lundbladh, A., and Johansson, A. V., 1991, "Direct simulation of turbulent spots in plane Couette flow", *Journal of Fluid Mechanics*, 229:499–516.

Mack, L. M., 1984, "Boundary-layer linear stability theory", Technical report AGARD No. 709, AGARD, Neuilly sur Seine, France.

Maeder, T., Adams, N. A., and Kleiser, L., 2001, "Direct simulation of turbulent supersonic boundary layers by an extended temporal approach", *Journal of Fluid Mechanics*, 429:187–216.

Maslowe, S. A., 1986, "Critical layers in shear flows", *Annual Review of Fluid Mechanics*, 18:405–432.

Schubauer, G. B., and Klebanoff, P. S., 1955, "Contributions to the mechanics of boundary layer transition", NACA-TN-3489.

Singer, B. A., 1996, "Characteristics of a young turbulent spot", *Physics of Fluids*, 8(2):509–521.

Singer, B. A., and Joslin, R. D., 1994, "Metamorphosis of a hairpin vortex into a young turbulent spot", *Physics of Fluids*, 6(11):3724–3736.

Stewartson, K., 1964, *"The Theory of Laminar Boundary Layers in Compressible Fluids"*, Claredon Press, Oxford.

Williamson, J. H., 1980, "Low-storage Runge-Kutta schemes", *Journal of Computational Physics*, 35:48–56.

Wygnanski, I., Haritonidis, J. H., and Kaplan, R. E., 1979, "On a Tollmien-Schlichting wave packet produced by a turbulent spot", *Journal of Fluid Mechanics*, 92:505–528.

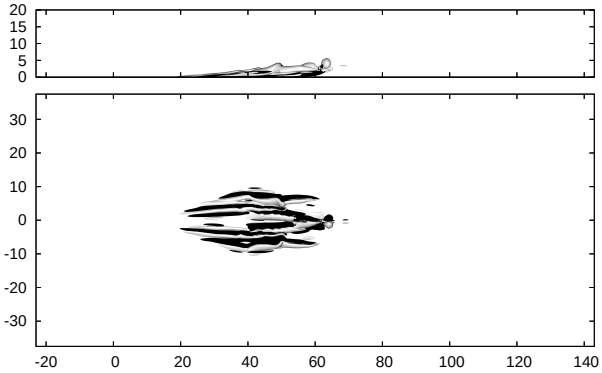

Figure 1: Iso-surfaces of $\omega_z = \pm 0.1$, single sample, case A1, $t = 77$.

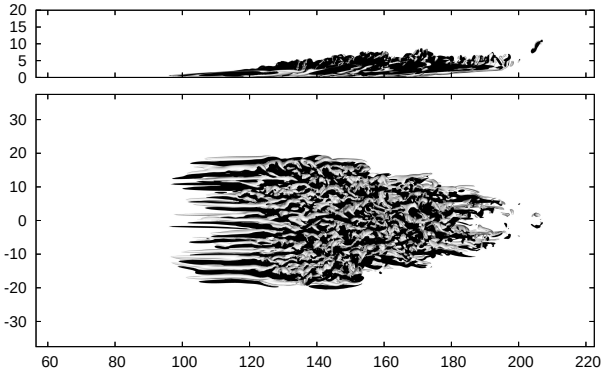

Figure 2: Iso-surfaces of $\omega_z = \pm 0.1$, single sample, case A1, $t = 228$.

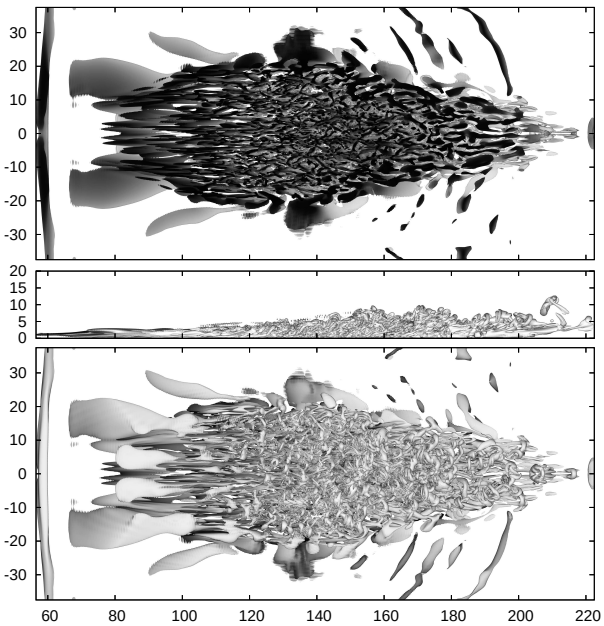

Figure 3: Iso-surfaces of λ_2, case A1, $t = 228$, bottom-view, mid-plane side-view, top-view. Bottom and top view are coloured with streamwise velocity, dark: low values, light: high values.

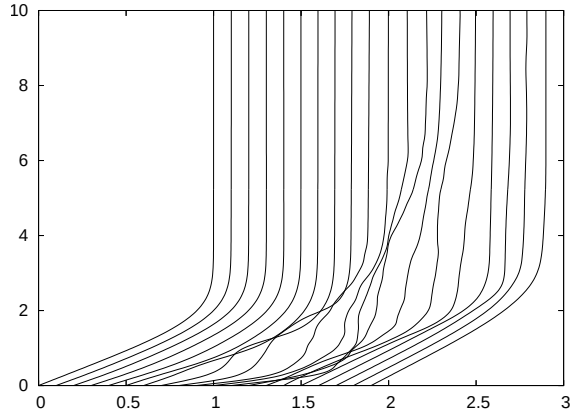

Figure 4: Profiles of Favre-averaged streamwise velocity $\tilde{u}$, case A1, $t = 228$.

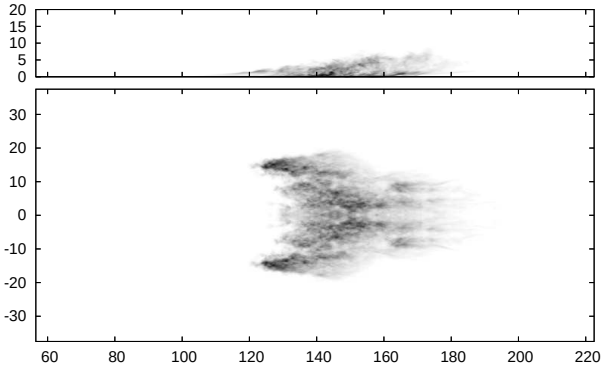

Figure 5: Reynolds normal stress $\bar{\rho}\widetilde{u''u''}$, case A1, $t = 228$, mid-plane side-view, $z = 3$-plane top-view, light: low values, dark: high values.

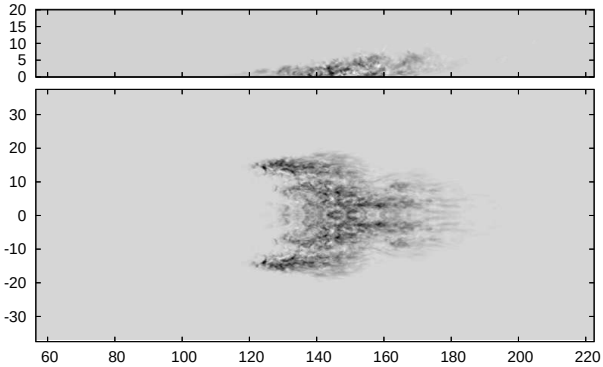

Figure 6: Reynolds shear stress $-\bar{\rho}\widetilde{u''w''}$, case A1, $t = 228$, mid-plane side-view, $z = 3$-plane top-view, light: low values, dark: high values.

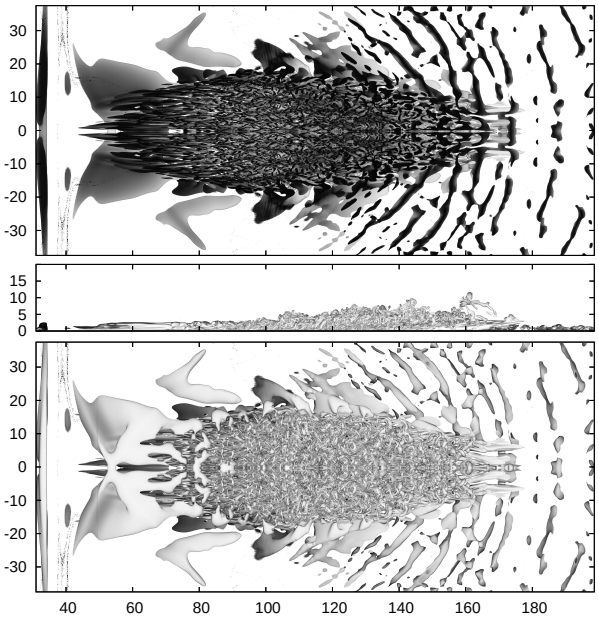

Figure 7: Iso-surfaces of λ_2, $M = 1.1$, $Re = 1500$, case A2, $t = 185$, arrangement as in Figure 3.

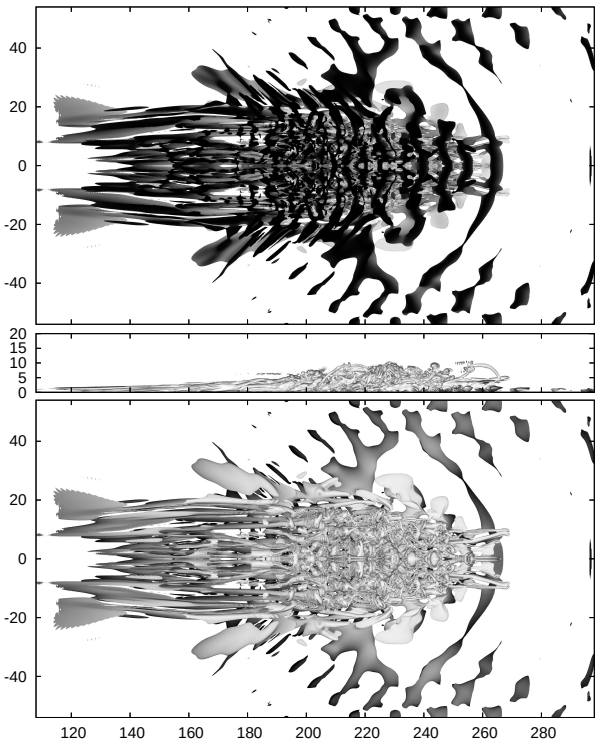

Figure 8: Iso-surfaces of λ_2, $M = 5$, $Re = 3000$, case B1, $t = 338$, arrangement as in Figure 3.

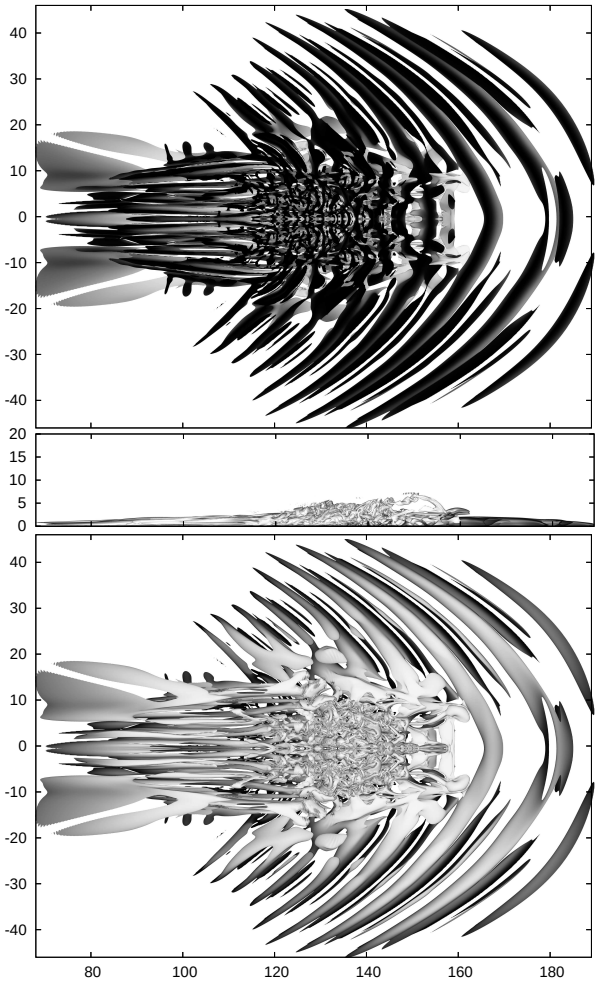

Figure 9: Iso-surfaces of λ_2, $M = 5$, $Re = 5000$, case B2, $t = 153.7$, arrangement as in Figure 3.

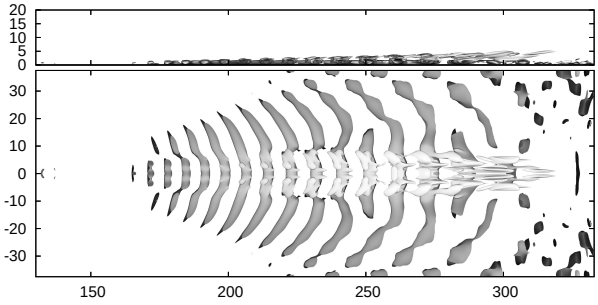

Figure 10: Iso-surfaces of λ_2, $M = 5$, $Re = 800$, $T_W = T_\infty$, case C, $t = 332$, mid-plane side-view and top-view.

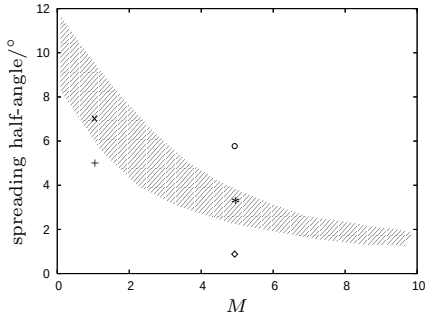

Figure 11: Spreading half-angle (estimated), + case A1, × case A2, ∗ case B1, ○ case B2, ◇ case C, shaded area experimental correlation of Fischer (1972).